Pergamon

Int. J. Heat Mass Transfer. Vol. 40, No. 17, pp. 4085–4094, 1997

Printed in Great Britain
0017–9310/97 $17.00+0.00

PII: S0017–9310(97)00062–8

Rapid solidification within the framework of a hyperbolic conduction model

ANDREW M. MULLIS
School of Materials, University of Leeds, Leeds LS2 9JT, U.K.

(*Received* 17 *October* 1996 *and in final form* 5 *February* 1997)

Abstract—Utilising high speed pulsed lasers, crystal growth velocities in excess of 250 m s^{-1} can be achieved in metallic systems. At such high growth rates it becomes pertinent to question the assumptions implicit within the Fourier model of thermal conduction. Specifically, the Fourier model allows an infinite velocity of propagation for heat. The rapid solidification problem is posed within a hyperbolic conduction model, imposing a finite velocity of propagation on the heat transfer process. We find that dendritic solidification is only possible if the growth velocity is less than half the thermal wave velocity, C. The likely value of C is discussed. © 1997 Elsevier Science Ltd.

1. INTRODUCTION

Fourier's model for the conduction of heat in solids is one of the most successful models utilized in the physical sciences. However, despite the excellent agreement between theory and experiment, the Fourier model possesses a pathological anomaly in that it implies an infinite velocity of propagation for heat. This anomaly is perhaps most apparent in the case of a semi-infinite solid subject to a step temperature change at its boundary, wherein Fourier's model predicts an instantaneous change in temperature at arbitrary distance from the boundary. In order to overcome this anomaly, Cattaneo [1] proposed a damped wave model for conduction in solids, whereby the heat conduction equation

$$\frac{\partial T}{\partial t} = \alpha \nabla^2 T \tag{1}$$

is modified by the addition of a wave-like component, to give a hyperbolic conduction equation

$$\frac{\partial T}{\partial t} + \tau \frac{\partial^2 T}{\partial t^2} = \alpha \nabla^2 T \tag{2}$$

where α is the thermal diffusivity in the liquid and τ is a thermal relaxation time. This model has the advantage that the 'heat wave' propagates with finite velocity C, where

$$C = \sqrt{\frac{\alpha}{\tau}} \tag{3}$$

and that for $t \gg \tau$, equation (2) reduces to the familiar Fourier heat conduction model. This is not to say that the hyperbolic conduction model is without its own conceptual difficulties. In particular, the wave-like nature of heat propagation leads to (transient) heat transfer against the direction of the imposed thermal gradient, in apparent contravention of the second law of thermodynamics. A number of recent papers have been aimed at addressing the problem of framing a hyperbolic conduction model in a way which is consistent with the second law [2]. Despite this, hyperbolic conduction models are widely regarded as preferable to the parabolic model for calculating the thermal response of media subject of step temperature change, at least for times $t \approx O(\tau)$, and an extensive literature has accumulated on the subject (see e.g. Joseph and Preziosi [3] for a comprehensive review of thought on heat waves).

Much of the work on hyperbolic heat conduction models has concentrated on calculating the transient response of a medium subject to a step temperature change. However, there is another class of problem on which hyperbolic conduction models may have a bearing, but which has received relatively little attention, that of a high velocity heat source moving through a medium. This problem has been considered by Tzou [4] in relation to the thermal field around a rapidly propagating crack tip, and will here be used to study the propagation of the solid–liquid interface during the rapid solidification of liquid metals.

The hyperbolic phase change problem was first considered by Sadd and Didlake [5], who considered the response of a semi-infinite one-dimensional solid subject to a step temperature change at its free boundary. They found that under these conditions the differences between the hyperbolic and parabolic models were restricted to times of the order 10^{-9}–10^{-11} s. Most subsequent work in this field [6–8] has concentrated on the correct formulation of the continuity conditions at the phase change boundary for the one-dimensional problem. In particular, Greenberg [7] has proposed that the continuity of temperature at the solid–liquid interface should be relaxed in hyperbolic

NOMENCLATURE

C	velocity of the thermal 'wave' [m s^{-1}]
c_p	specific heat capacity [J kg^{-1} K^{-1}]
G	thermal gradient at the solid/liquid interface [K m^{-1}]
H	latent heat on fusion [J kg^{-1}]
M	molar mass [kg mol^{-1}]
$\hat{n}$	outward normal to the solid liquid interface
P	thermal Peclet number
R	gas constant [J mol^{-1} K^{-1}]
R	radius of curvature at the dendrite tip [m]
r	cylindrical co-ordinate direction [m]
T	temperature [K]
T_i	local interface (liquidus) temperature [K]
T_m	equilibrium liquidus temperature [K]
T_∞	temperature far from the solid/liquid interface [K]
t	time [s]
V_s	velocity of sound in the liquid [m s^{-1}]
V	growth velocity of an isolated dendrite
V_0	dendrite growth velocity in an isotropic liquid [m s^{-1}]
V_h	dendrite growth velocity in the hyperbolic conduction model [m s^{-1}]
V_{max}	maximum dendrite growth velocity in the hyperbolic model [m s^{-1}]
V_p	dendrite growth velocity in the conventional (parabolic) conduction model [m s^{-1}]
x	Cartesian co-ordinate direction [m]
y	Cartesian co-ordinate direction [m]
z	Cartesian/cylindrical co-ordinate direction [m].

Greek symbols

α	thermal diffusivity [m^2 s^{-1}]
α_z	thermal diffusivity in the growth direction [m^2 s^{-1}]
ΔT	total undercooling [K]
ΔT_k	kinetic undercooling [K]
ΔT_{max}	maximum undercooling at which growth is stable (hyperbolic model) [K]
ΔT_r	curvature undercooling [K]
ΔT_t	thermal undercooling [K]
δV	relative velocity difference between hyperbolic and parabolic models
Γ	Gibbs–Thomson parameter [K m]
γ	interfacial energy between solid and liquid phases [J m^{-2}]
η	dimensionless parabolic co-ordinate direction
ϑ	dimensionless temperature
κ	thermal conductivity [W m^{-1} K^{-1}]
$\bar{\kappa}$	reduced thermal conductivity
θ	angle between outward normal to interface and principal growth direction [rad]
ρ	density [kg m^{-3}]
σ^*	stability constant
τ	thermal relaxation time (hyperbolic model) [s]
ξ	dimensionless parabolic co-ordinate direction.

Subscripts

i	quantities internal to the freezing front
e	quantities external to the freezing front
l	properties of the liquid
s	properties of the solid.

phase-change models, leading to a discontinuity in the temperature at the interface. This idea has been developed by Glass *et al.* [8], who derive an interface continuity equation relating the interface temperature in the liquid to the interface temperature in the solid, in terms of the interface velocity and acceleration.

The value of C, or conversely τ, in metallic systems is a matter of some conjecture. Brazel and Nolan [9] estimate τ for metals to be in the range 10^{-10}–10^{-12} s, which accords with estimates made by Baumeister and Hamill [10] that C is of the order 1000 m s^{-1}. On the basis of an analysis of quantum scattering processes Maurer [11] suggests that $\tau \approx 10^{-11}$–10^{-14} s. However, such analyses are perhaps somewhat simplistic. Joseph and Preziosi [3] argue that τ can be modelled as a kernel consisting of two (or more) components, a fast one of order 10^{-14} s, and a slow one of order 10^{-11} s. These may correspond to conduction limited by different scattering processes. In this model the effective value of τ is determined by the dominant scattering process.

Evidence in support of the existence of heat waves is provided by the existence of second sound in helium [12]. In addition to the propagation of conventional sound wave through helium, Landau detected the presence of a second, slower, wave, which is associated with the propagation of the thermal disturbance. The velocity of second sound varied from $V_s/\sqrt{3}$ at 4K to zero at the triple point. Second sound has never been detected in high temperature solids, but simulations of the dynamics of a crystal lattice [13] indicate that a thermal perturbation applied to one side of the crystal did indeed propagate through the lattice in a wave like manner at a velocity of $V_s/\sqrt{3}$. Most liquid metals have velocities of sound in the range 2000–4000 m s^{-1}, giving $V_s/\sqrt{3}$ in the range 1000–2000 m s^{-1}.

The rapid solidification of a metallic melt can be occasioned by one of two routes; by inhibiting hetero-

geneous nucleation, so that bulk undercooling of the specimen can be achieved, or by utilizing very high cooling rates, which involves making one of the sample dimensions very small. For the former method, containerless processing techniques (drop tube processing or electromagnetic levitation in an inert atmosphere) allow samples to be cooled to $\approx 70\%$ of their absolute melting temperature without solidification being nucleated (see e.g. Herlach *et al.* [14] for a review of containerless processing techniques). Once nucleated, solidification proceeds by way of a dendritic front which grows into the liquid at a constant velocity determined by the rate at which excess heat can be diffused into the undercooled liquid. In rapid quenching experiments the use of high power pulsed laser to melt thin films (≈ 100 nm) allows cooling rates in excess of 10^{12}K s^{-1} to be achieved. Such high cooling rates strongly inhibit nucleation in the liquid [15] producing a highly undercooled liquid. Solidification thus proceeds via the same route as for a bulk undercooled sample, with the solid–liquid interface velocity being determined by the rate of heat rejection into the liquid. Using such techniques interface velocities of 250 m s^{-1} may be achieved [16].

The rapid solidification of materials with a low entropy of transformation between the liquid and solid states, such as most metals, occurs via the growth of dendrites. These are needle-like crystals which, to a good approximation, are parabolic at the tip [17] and which propagate through the melt at constant velocity. The growth of these features is conventionally modelled by converting to a frame of reference co-moving with the dendrite tip, wherein the problem can be considered in a quasi-steady state manner. Solutions to the resulting equations can be obtained by converting to a parabolic co-ordinate system [18]. In this paper we give a brief overview of this analysis from the starting point of the conventional Fourier conduction model and then compare this with the results of starting from a hyperbolic conduction model. As the resulting hyperbolic equations do not appear amenable to analytical solution a numerical model [19] is used to compare the behaviour of the Fourier and hyperbolic solutions.

Before considering the detailed mathematical formulation of the rapid solidification problem, some preliminary observations may be made. The velocity at which the solid–liquid interface propagates is limited by a number of factors including the rate at which heat is diffused away from the interface into the liquid. Thus, we can deduce immediately that C will be an absolute upper limit to the rate of progress of the front. This will be significant if $C < V_s$, the velocity of sound in the liquid, which has previously been taken as the upper limit to the interface velocity [20]. V_s being the maximum velocity at which atomic rearrangement can occur to form the crystalline solid.

The rapid solidification problem is thus fundamentally different to that of crack propagation studied by Tzou [4], as the crack velocity is not limited by the rate at which thermal energy is removed from the crack tip. In fact, Tzou considers both subsonic ($V < C$) and supersonic ($V > C$) crack propagation.

2. MATHEMATICAL FORMULATION OF THE RAPID SOLIDIFICATION PROBLEM

The progress of a quasi-steady state solidification front moving at constant velocity V can be modelled by converting to a co-moving co-ordinate system. Taking V to be aligned along the z direction, the moving co-ordinate system (x', y', z') can be related to the laboratory frame (x, y, z) by

$$x' = x, \quad y' = y, \quad z' = z - V_t. \tag{4}$$

Under this transformation all spatial derivatives, including $\partial^n/\partial z'^n$, are invariant, but the first and second time derivatives transform as

$$\frac{\partial}{\partial t} = \frac{\partial}{\partial t'} - V\frac{\partial}{\partial z'} \tag{5a}$$

$$\frac{\partial^2}{\partial t^2} = \frac{\partial}{\partial t'^2} - 2V\frac{\partial^2}{\partial t'\,\partial z'} + V^2\frac{\partial^2}{\partial z'^2}. \tag{5b}$$

Substituting equation (5a) into equation (1) and taking $\partial T/\partial t' = 0$ yields

$$\nabla^2 T + \frac{V}{\alpha}\frac{\partial T}{\partial z} = 0 \tag{6}$$

where we have now dropped the $'$ superscript, as all subsequent equations are written in co-moving co-ordinates. Equation (6) is sometimes referred to as the directional solidification equation. Substitution of equations (5a, b) into equation (2) yields the hyperbolic equivalent of the directional solidification equation, namely

$$\nabla^2 T + \frac{V}{\alpha}\frac{\partial T}{\partial z} - \frac{\tau V^2}{\alpha}\frac{\partial^2 T}{\partial z^2} = 0. \tag{7}$$

Note that in a moving co-ordinate system τ enters not only into the transient, but also the quasi-steady-state equation. This results in a velocity dependant diffusivity anisotropy in the liquid, with the diffusivity in the direction of propagation, α_z, being a minimum.

$$\alpha_z = \alpha\left(1 - \frac{\tau V^2}{\alpha}\right) = \alpha\left(1 - \frac{V^2}{C^2}\right). \tag{8}$$

For most pure metals, and other systems that freeze with a low entropy of transformation, solidification into the undercooled liquid commonly proceeds via dendritic growth. To a very good approximation, the tip of a dendritic needle crystal can be modelled as a parabolic plate for two-dimensional solidification or as a paraboloid of revolution in three-dimensions [17]. Solutions to the (Fourier) directional solidification equation are thus obtained by transforming to dimensionless, co-moving, parabolic co-ordinates (ξ, η). In two-dimensions

$$\xi^2 = \frac{\sqrt{x^2+z^2}+z}{R}, \quad \eta^2 = \frac{\sqrt{x^2+z^2}-z}{R} \tag{9a}$$

while for three-dimensional solidification, the rotational symmetry of the freezing front allows the dimension of the problem may be reduced by one by transforming to cylindrical co-ordinates (r, ϕ, z), wherein

$$\xi^2 = \frac{\sqrt{r^2+z^2}+z}{R}, \quad \eta^2 = \frac{\sqrt{r^2+z^2}-z}{R} \tag{9b}$$

where R is the radius of curvature of the dendrite tip. In parabolic co-ordinates, lines of constant ξ are concentric paraboli, while η is a running co-ordinate along the parabola. Under this transformation the differentials may be written

$$\frac{\partial}{\partial x} = \frac{\partial}{\partial r} = \frac{1}{R(\xi^2+\eta^2)}\left(\eta\frac{\partial}{\partial \xi} + \xi\frac{\partial}{\partial \eta}\right) \tag{10a}$$

$$\frac{\partial}{\partial z} = \frac{1}{R(\xi^2+\eta^2)}\left(\xi\frac{\partial}{\partial \xi} - \eta\frac{\partial}{\partial \eta}\right). \tag{10b}$$

Thus, equation (6) transforms to

$$J_2(\xi,\eta) = \frac{\partial^2 \vartheta}{\partial \xi^2} + \frac{\partial^2 \vartheta}{\partial \eta^2} + 2P\left(\xi\frac{\partial \vartheta}{\partial \xi} - \eta\frac{\partial \vartheta}{\partial \eta}\right) = 0 \tag{11}$$

in two-dimensions and

$$J_3(\xi,\eta) = \frac{\partial^2 \vartheta}{\partial \xi^2} + \frac{\partial^2 \vartheta}{\partial \eta^2} + \frac{\partial \vartheta}{\xi\,\partial\,\xi} + \frac{\partial \vartheta}{\eta\,\partial\,\eta} + 2P\left(\xi\frac{\partial \vartheta}{\partial \xi} - \eta\frac{\partial \vartheta}{\partial \eta}\right) = 0 \tag{12}$$

in three-dimensions, where ϑ is the dimensionless temperature

$$\vartheta = \frac{c_p}{H}(T - T_\infty) \tag{13}$$

P the thermal Peclet number,

$$P = \frac{VR}{2\alpha} \tag{14}$$

c_p the specific heat capacity, H the latent heat on fusion, and T_∞ the temperature at large distance from the freezing front. Boundary conditions are provided in the far field by

$$\vartheta \underset{\xi\to\infty}{\to} 0 \tag{15}$$

and at the freezing front, $\xi = 1$, by continuity of the temperature and heat-flux at the solid–liquid interface

$$\vartheta_e = \vartheta_i \tag{16a}$$

$$\rho HV\cos\vartheta = \kappa_s\frac{\partial \vartheta_i}{\partial \hat{n}} - \kappa_l\frac{\partial \vartheta_e}{\partial \hat{n}} \tag{16b}$$

where the subscripts e and i refer to quantities external and internal to the freezing front, respectively, $\hat{n}$ is the dimensionless unit surface normal to the freezing front, θ the angle between $\hat{n}$ and the principal growth direction, κ_l and κ_s the thermal conductivities in the liquid and solid and ρ the density, considered to be the same in the solid and liquid states to avoid consideration of density driven flow effects. Note that in the quasi-steady-state case the simple continuity of temperature condition expressed by equation (16a) is appropriate for the hyperbolic, as well as the parabolic, phase change model. As formulated by Glass *et al.* [8], letting $\dot{V}$, $\dot{\vartheta}_e$ and $\dot{\vartheta}_i$ go to zero in the interface continuity condition for hyperbolic phase change (their equation 10), is equivalent to the limit $\tau \to 0$.

Both equations (11) and (12) are separable, yielding solutions,

$$\vartheta = \sqrt{\pi P_t}\exp(P)\,\mathrm{erfc}(\sqrt{P\xi}) \tag{17}$$

in two-dimensions and

$$\vartheta = -P_t\exp(P)\mathrm{Ei}(-P\xi^2) \tag{18}$$

in three-dimensions. Here erfc is the complimentary error function and Ei the exponential integral function. Rigorous analysis of this problem is provided by Ivantsov [18] and Horvay and Cahn [21].

In both two- and three-dimensions the solutions for ϑ are degenerate with respect to V. However, in nature a unique solidification velocity is associated with a given undercooling. Hence some additional, scale dependant, mechanism must operate to select an appropriate value of R and hence V from the infinite set of admissible solutions represented by the condition VR = constant. The simplest such condition is that of marginal stability, which holds that the dendrite with the largest unstable wavelength is the one which will predominate. For growth at arbitrary Peclet number this is [22],

$$R^2 = \frac{-\Gamma}{\sigma^*(\kappa_s\zeta_s G_s + \kappa_l\zeta_l G_l)} \tag{19}$$

with

$$\overline{\kappa_s} = \frac{\kappa_s}{\kappa_s+\kappa_l}, \quad \overline{\kappa_l} = \frac{\kappa_l}{\kappa_s+\kappa_l} \tag{20}$$

$$\zeta_l = 1 - \frac{1}{(1+(2\pi/P_l)^2)^{1/2}}, \quad \zeta_s = 1 + \frac{1}{(1+(2\pi/P_s)^2)^{1/2}} \tag{21}$$

where P_l and P_s are the thermal Peclet numbers in the liquid and solid, which may be different because of the different thermal diffusivities, Γ is the Gibbs–Thomson parameter

$$\Gamma = \frac{\gamma T_m}{\rho H} \tag{22}$$

T_m the equilibrium liquidus temperature, γ the interfacial energy between the solid and liquid phases and

G the (dimensional) normal thermal gradient at the tip. σ^* is a stability constant which for a plane interface [23] takes the value $1/4\pi^2$.

However, even for a pure metal, curvature and kinetic effects will depress the local liquidus temperature below its equilibrium value, leading to a reduction in the effective undercooling. This can be included in the calculation by writing the total undercooling at the dendrite surface as

$$\Delta T = \Delta T_t + \Delta T_r + \Delta T_k \tag{23}$$

where ΔT_t is the thermal undercooling at the dendrite surface, that is the difference between the local interface temperature T_i and the far field temperature T_∞, ΔT_r is the Gibbs–Thomson (curvature) undercooling given by

$$\Delta T_r = \frac{2\Gamma}{R} \tag{24}$$

and ΔT_k is a kinetic undercooling [20]

$$\Delta T_k = \frac{1000 R T_m^2}{V_s M H} V \tag{25}$$

where M is the molar mass and R is the gas constant. When curvature and kinetic effects are included the non-equilibrium growth model described by equations (17)–(25) is found to be in reasonable agreement with experimentally determined growth velocity data for pure metals [24, 25], over the range of velocities for which data is currently available. However, many of the fundamental features of dendritic growth can be deduced by considering the simpler equilibrium model.

The hyperbolic equivalents of equations (11) and (12) are

$$J_{(2,3)}(\xi,\eta) - \frac{\tau V^2}{\alpha} K(\xi,\eta) = 0 \tag{26}$$

where

$$K(\xi,\eta) = \frac{1}{(\xi^2+\eta^2)}\left(\xi^2\frac{\partial^2\vartheta}{\partial\xi^2} - 2\xi\eta\frac{\partial^2\vartheta}{\partial\xi\,\partial\eta} + \eta^2\frac{\partial^2\vartheta}{\partial\eta^2} + \xi\left(\frac{3\eta^2-\xi^2}{\xi^2+\eta^2}\right)\frac{\partial\vartheta}{\partial\xi} + \eta\left(\frac{3\xi^2-\eta^2}{\xi^2+\eta^2}\right)\frac{\partial\vartheta}{\partial\eta}\right). \tag{27}$$

These equations are not separable in either two- or three-dimension. Thus, in order to assess the effect on dendritic growth of the diffusivity anisotropy introduced by the hyperbolic conductivity model we have solved equation (7) numerically for the temperature field around the growing dendrite. The solution is obtained using standard finite element techniques utilizing a triangular grid, consisting of M rows, each of N nodes. For a parabolic freezing front rows of nodes are arranged along lines of constant ξ while columns of nodes are arranged along lines of constant η. From the solution to equation (7) the thermal gradients G_i and G_e and hence V and R can be evaluated. The updated values of V and R are used to re-evaluate the temperature of the freezing front using equations (23)–(25), thus defining an iterative procedure in which equation (7) is repeatedly solved until successive values of V and R converge to within an acceptable tolerance. This model is described in greater detail (for Fourier thermal conduction) elsewhere [19].

3. RESULTS AND DISCUSSION

Figure 1 compares the calculated hyperbolic growth velocities, V_h, for dendrites in two- and three-dimen-

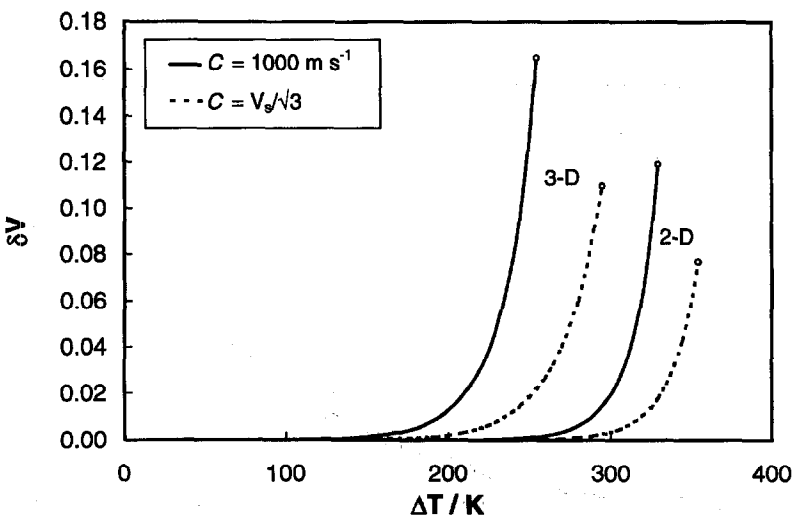

Fig. 1. Dendritic growth velocity within the hyperbolic conduction model relative to that in the conventional Fourier conduction model for dendrites in two- and three-dimensions as a function of undercooling, Δt. The quantity δV is defined as $\delta V = (V_h - V_p)/V_p$ where V_h is the hyperbolic growth velocity and V_p the parabolic (Fourier) growth velocity. The calculation is performed within the equilibrium solidification model described in the text, for dendrites growing in liquid Ni.

Table 1. Material parameters for nickel and copper

Parameter	Symbol	Ni	Cu	Units	Reference
Melting temperature	T_m	1726	1356	K	24
Specific heat capacity	c_p	655.7	493.9	$J\,kg^{-1}\,K^{-1}$	24
Latent heat on melting	H	292200	204900	$J\,kg^{-1}$	24
Density of liquid	ρ	7905	8000	$kg\,m^{-3}$	25
Thermal conductivity of solid	κ_s	82.50	160	$W\,m^{-1}\,K^{-1}$	26
Thermal conductivity of liquid	κ_l	58.90	397	$W\,m^{-1}\,K^{-1}$	26
Solid–liquid interfacial energy	γ	0.367	0.223	$J\,m^{-2}$	27
Velocity of sound	V_s	4036	3450	$m\,s^{-1}$	20

sions, with the velocity derived from the equivalent parabolic model, V_p, as a function of undercooling. The calculation has been performed using the data typical of Ni, which is given in Table 1. In the first instance we have performed the calculation within the equilibrium freezing model, that is the effects of curvature and attachment kinetics (ΔT_r and ΔT_k) have not been included in the calculation. This is done in order that we may distinguish features that arise as a fundamental consequence of the growth of dendrites within a hyperbolic conduction model from those which are due to the action of the curvature and kinetic terms. This model will subsequently be compared with the full non-equilibrium model. As, over most of the undercooling range studied, V_h and V_p are so close as to be virtually indistinguishable, the comparison is, for clarity, made by plotting

$$\delta V = \frac{V_h - V_p}{V_p}. \tag{28}$$

Note that strictly δV does not exist at $\Delta T = 0$ as both V_p and $V_h = 0$. However, it is clear from the data that in the limit $\Delta T \to 0$ we have $\delta V \to 0$.

Two principal observations can be made regarding the results of these simulations. Firstly, the growth velocity within the hyperbolic model is always faster than that for the conventional solution ($\delta V > 0$). This is perhaps somewhat surprising as, from equation (8), we deduce that the effective thermal diffusivity in the growth direction is reduced relative to its nominal value. We might, therefore, expect the growth velocity to be reduced commensurately. Secondly, as ΔT approaches some limit, ΔT_{max}, the hyperbolic velocity rapidly becomes very much faster than the equivalent parabolic velocity. Above this limit, which is variable between simulations depending upon the parameters used, the solution within the hyperbolic model appears not to exist. For each simulation, the approximate location of ΔT_{max} is shown in Fig. 1 by an open circle at the end of the curve. Strictly ΔT_{max} may occur at slightly higher undercooling than indicated, as the open circle actually indicates the highest undercooling for which a solution could be obtained, with ΔT being incremented in steps of 5K.

The behaviour of the solutions is further explored in Fig. 2, in which the results have been replotted as a function of V_p/C. From this figure it is clear that although ΔT_{max} is variable between simulations, the ratio V_p/C above which we were unable to find solutions appears approximately constant at $V_{max}/C \approx 0.45$,

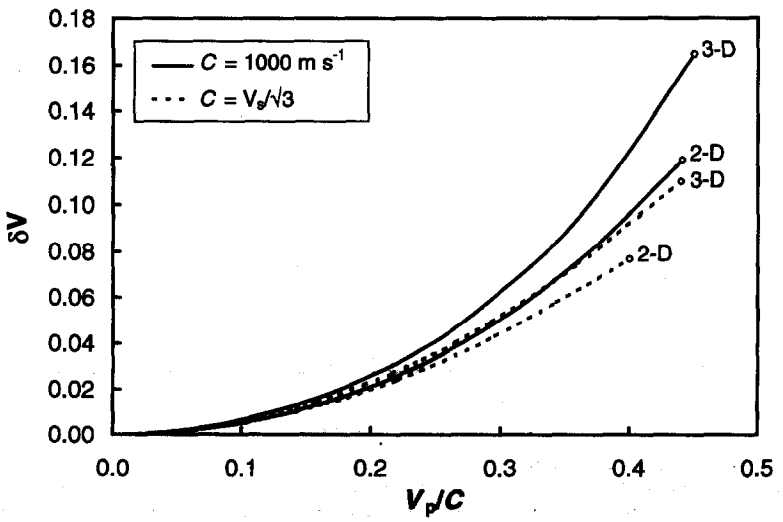

Fig. 2. Dendritic growth velocity within the hyperbolic conduction model relative to that in the conventional Fourier conduction model for dendrites in two- and three-dimensions as a function of the ratio V_p/C.

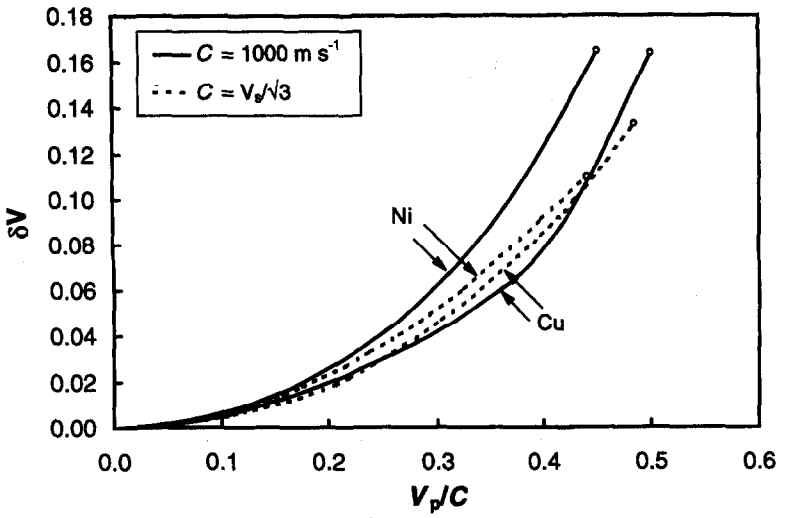

Fig. 3. Dendritic growth velocity within the hyperbolic conduction model relative to that in the conventional Fourier conduction model for dendrites growing in Ni and Cu.

where V_{max} is the value of V_p corresponding to an undercooling of ΔT_{max}. Again the last point on the curve is denoted by an open circle to indicate that this is the entire range over which the solution exists.

These conclusions appear relatively insensitive to the choice of material parameters, as illustrated in Fig. 3, where we compare the results for Ni with those for Cu. The solutions for Cu exist over a slightly higher range of values of V_p/C, with V_{max} occurring near $0.5C$, but the general form of the curves is similar. Preliminary results for simulations with other pure metals (Fe, Co, Ag and Au) also show a similar pattern, which lead us to believe that the results obtained are typical of dendritic solidification within a hyperbolic conduction model, irrespective of the material being solidified.

Simulations have also been performed for the full non-equilibrium model, which include curvature and kinetic effects (Fig. 4). Again we find a broadly similar pattern of results, with $\delta V > 0$ for all $\Delta T > 0$ and solutions which exist only if $V_p \leqslant V_{max} \approx C/2$. The curve for the non-equilibrium simulation is flatter at low growth velocities than the equivalent equilibrium curve with an elbow at close to $V_p/C = 0.5$, beyond which δV increases rapidly. These differences between the simulations appear to result mainly from the effect of the kinetic term, ΔT_k [equation (25)]. In the non-equilibrium simulation there is a complex interaction between the hyperbolic term (proportional to V^2) which is promoting faster growth by lowering the thermal diffusivity in the growth direction and the kinetic term (proportional to V) which is suppressing the growth velocity by depressing the interface temperature.

As shown by equation (8) the effect of introducing a hyperbolic conduction term into the directional solidification equation is to produce a velocity dependant anisotropy in α. As there has previously been little motivation to investigate dendritic growth into an anisotropic liquid we now consider the effect of a uniform anisotropy in the growth (z) direction, in order to understand the results of the hyperbolic simulations. Let the thermal diffusivity in the growth direction be

$$\alpha_z = (1-\varepsilon)\alpha \tag{29}$$

with $0 \leqslant \varepsilon \leqslant 1$. In Fig. 5 we show the growth velocity of a parabolic dendrite at fixed undercooling ($\Delta T = 100$K) as a function of ε, within the equilibrium growth model. The calculation is performed for Ni. For $\varepsilon \to 0$, V is proportional to ε, suggesting, somewhat paradoxically, that as the thermal diffusivity in the growth direction decreases, growth velocity increases. This can be understood as a consequence of the marginal stability hypothesis [equation (19)], in which the thermal gradient at the tip determines the curvature. The reduced thermal diffusivity in the growth direction leads to a higher thermal gradient at the tip and hence smaller tip size. In fact, as shown in Fig. 6, at a fixed undercooling R decreases linearly with ε. Thus if the hyperbolic solution behaved in all other respects in exactly the same way as the conventional Fourier solution we would expect a commensurate increase in V such that the product VR remained constant [see equations (17) and (18)]. In fact, the product VR decreases slightly with increasing ε due to the decreased efficiency of heat transfer away from the tip, but this is a minor effect and the tendency is for V to still increase with ε.

We now consider an order of magnitude argument to elucidate the origin of the instability above $V_{max}/C \approx 0.5$. From Fig. 5 we deduce that, for small values of ε, an anisotropic diffusivity $\alpha_z = \alpha(1-\varepsilon)$ gives rise to a velocity $V = V_0(1+\varepsilon)$, V_0 being the velocity corresponding to $\varepsilon = 0$. Within the hyperbolic model the anisotropy is given by V^2/C^2. Thus, provided V is close to V_0, in the hyperbolic model we have,

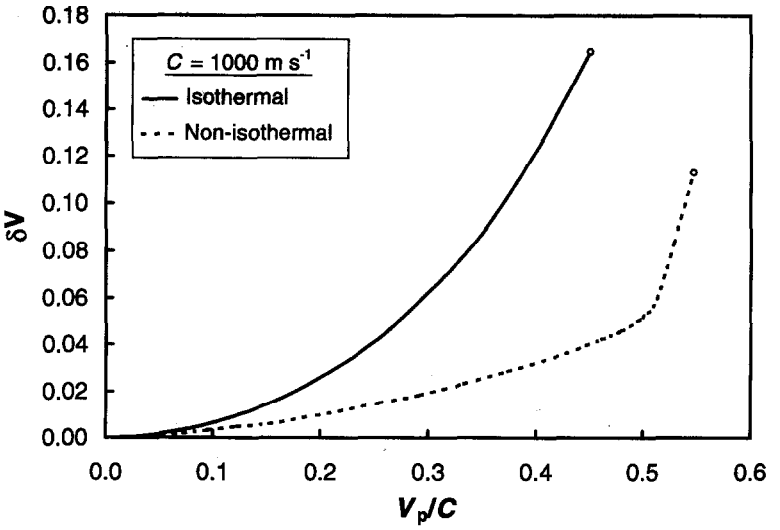

Fig. 4. Comparison of the dendritic growth velocity within the hyperbolic conduction model relative to that in the conventional Fourier conduction model for the equilibrium and non-equilibrium solidification model discussed in the text.

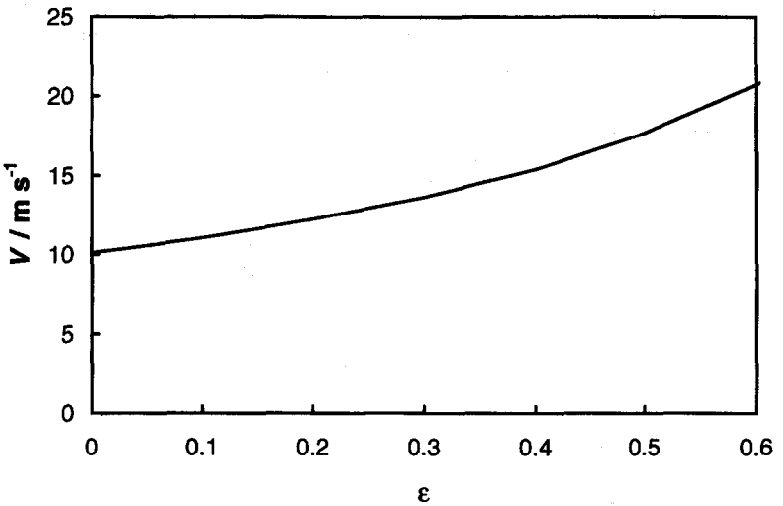

Fig. 5. Growth velocity for a dendrite growing into a liquid with anisotropic thermal conductivity, $\alpha_2 = \alpha(1-\varepsilon)$. Calculation performed at a fixed undercooling of $\Delta T = 100$ K.

$$V = V_0\left(1+\frac{V^2}{C^2}\right). \tag{30}$$

Roots to the quadratic only exist provided $V_0 \leqslant C/2$. Physically we interpret this as a manifestation of the 'positive feedback' coupling between V and α_z. As the velocity increases, α_z decreases, and there is a tendency for V to increase further. Beyond $V \approx C/2$ this coupling appears to be so strong that the system becomes unstable and the solution ceases to exist. It is not clear, however, what mode of growth, if any, exits beyond $V_0 \approx C/2$.

4. CONCLUSION

From the above analyses we conclude that within the framework of a hyperbolic conduction model the growth of a dendritic needle crystal is always faster than in the equivalent Fourier model. This result appears, at first sight, paradoxical as introducing a finite thermal wave velocity into the steady state growth equation leads to a velocity dependant reduction in the thermal diffusivity in the principal growth direction. This result can be understood as a consequence of the radius of curvature at the dendrite tip being a function of the thermal gradient at the tip. The higher thermal gradients encountered in the hyperbolic model lead to a smaller tip size and hence faster growth. Above $V \approx C/2$ the increased growth velocity results in a runaway instability with the apparent loss of existence of the needle dendrite solutions to the directional growth equation.

For $V < C/2$ the increase in growth velocity associ-

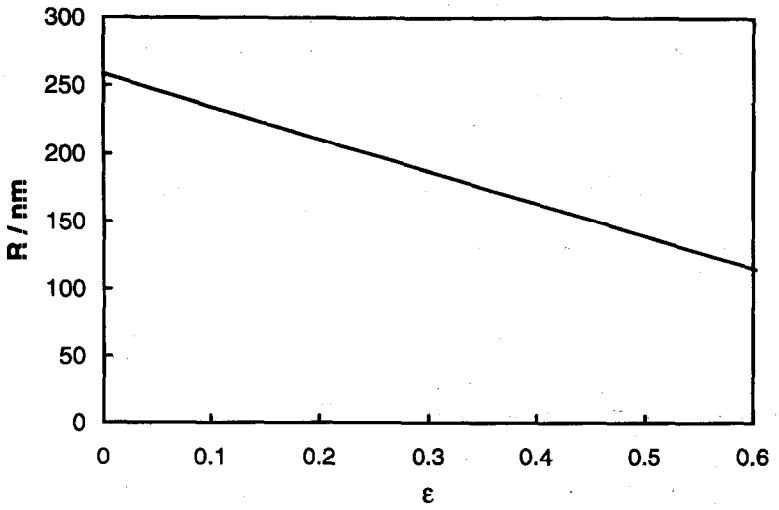

Fig. 6. Radius of curvature at the tip for a dendrite growing into a liquid with anisotropic thermal conductivity, $\alpha_z = \alpha(1-\varepsilon)$. Calculation performed at a fixed undercooling of $\Delta T = 100$K.

ated with the hyperbolic solutions is small and consequently it is very unlikely that the finite velocity of thermal propagation will be detectable in rapid solidification experiments. Any effect is likely to be masked by the experimental error involved in making the measurements, or overlooked due to the difficulty in accurately modelling V as a function of ΔT. However, if it is possible to approach $C/2$, then a clear and dramatic change in solidification morphology should occur, this being associated with the runaway instability in V, apparent in the needle dendrite solutions to the hyperbolic heat conduction equation. From this analysis it is not clear what morphology might replace dendritic growth above $V_{max} \approx C/2$, or indeed even if solidification at velocities exceeding V_{max} is possible.

The likelihood of such effects being observed depends critically on the value of C. If C is as low as 1000 m s^{-1}, the fastest recalescence events yet recorded are only a factor of two below V_{max}, with the possibility that improved processing techniques will lead to V_{max} being approached in the near future. However, if C is significantly higher than 1000 m s^{-1} the possibility of V approaching V_{max} is correspondingly reduced. In Ni, $V_s \approx 4000$ m s^{-1} [26], so associating C with $V_s/\sqrt{3}$ we have $C = 2300$ m s^{-1} and $V_{max} = 1150$ m s^{-1}. This is more than four times the highest interface velocity recorded, but with improvements in high speed laser technology still perhaps not unattainable.

If these effects are to be observed it is likely that it will be in rapid laser melting experiments, where the high post-recalescence rate of heat extraction ensures that the original solidification microstructure is 'frozen in'. With techniques such as electromagnetic levitation high values of ΔT can be achieved but the rate of post-recalescence heat extraction is low, allowing significant time for evolution of the solidification microstructure. This has been observed to lead to remelting effects in a number of pure metals and alloys at high undercooling [24, 25, 27].

Acknowledgements—The author is grateful to the Royal Society for their generous support under the University Research Fellowship scheme.

REFERENCES

1. Cattaneo, C., Sulla conduzione de calore. *Atti del Seminario Mathematica e Fisico della Universitata di Modena*, 1948, **3**, 3–21.
2. Bai, C. and Lavine, A. S., On hyperbolic conduction and the 2nd law of thermodynamics. *Journal of Heat Transfer*, 1995, **117**, 256–263.
3. Joseph, D. D. and Preziosi, L., Heat waves. *Review of Modern Physics*, 1989, **61**, 41–73.
4. Tzou, D. Y., Thermal shock waves induced by a moving crack. *Journal of Heat Transfer*, 1990, **112**, 21–27.
5. Sadd, M. H. and Didlake, J. E., Non-Fourier melting of a semi-infinite solid. *Journal of Heat Transfer*, 1977, **99**, 25–28.
6. Solomon, A. D., Alexiades, V., Wilson, D. G. and Drake, J., On the formulation of hyperbolic Stefan problems. *Quarterly Applied Mathematics*, 1985, **3**, 295–304.
7. Greenberg, J. M., A hyperbolic heat transfer problem with phase changes. *IMA Journal of Applied Mathematics*, 1997, **38**, 1.
8. Glass, D. E., Ozisik, M. N., McRae, S. S. and Kim, W. S., Formulation and solution of hyperbolic Stefan problems. *Journal of Applied Physics*, 1991, **70**, 1190–1197.
9. Brazel, J. P. and Nolan, E. J., Non-Fourier effects in the transmission of heat. *Proceedings of the Sixth Conference on Thermal Conductivity*, Dayton, Ohio, 1966, ed. M. L. Minges and G. L. Denman, 1967, pp. 237–254.
10. Baumeister, K. J. and Hamill, T. D., Hyperbolic heat conduction equation—a solution for the semi-infinite body problem. *Journal of Heat Transfer*, 1969, **91**, 543–548.
11. Maurer, M. J., Relaxation model for heat conduction in metals. *Journal of Applied Physics*, 1969, **40**, 5123–5130.
12. Landau, L., The theory of superfluidity in liquid helium II. *Journal of Physics*, 1941, **5**, 71.

13. Tsai, D. H. and MacDonald, R. A., Molecular dynamical study of second sound in a solid excited by a strong heat pulse. *Physics Review*, 1976, **B14,** 4714–4723.
14. Herlach, D. M., Cochrane, R. F., Egry, I., Fechy, H. J. and Greer, A. L., Containerless processing in the study of metallic melts and their solidification. *International Materials Review*, 1993, **38,** 273–347.
15. Stiffler, S. R., Thompson, M. O. and Peercy, P. S., Transient nucleation following pulsed laser melting of thin silicon films. *Physics Review B*, 1991, **43,** 9851–9855.
16. Aziz, M. J., Non-equilibrium interface kinetics during rapid solidification. *Materials Science Engineering*, 1994, **A178,** 167–170.
17. Papapetrou, A., Untersuchunge über dendritisches wachstum von kristallen. *Zeitschrift Kristallographie*, 1935, **82,** 89–130.
18. Ivantsov, G. P., *Doklady Adkademie Nauka SSSR*, 1947, **58,** 567–569. Translation available as *General Electronics Research Laboratory Report* 60-RL-2511M.
19. Mullis, A. M., A free boundary model for shape preserving dendritic growth at high undercooling. *Journal of Applied Physics*, 1996, **80,** 4129–4136.
20. Turnbull, D., Relative roles of heat transport and interface rearrangement rates in the rapid growth of crystals in undercooled melts. *Acta Metallurgica*, 1982, **30,** 2135–2139.
21. Horvay, G. and Cahn, J. W., Dendritic and spheroidal growth, *Acta Metallurgica*, 1961, **9,** 695–705.
22. Lipton, J., Kurz, W. and Trivedi, R., Rapid dendritic growth in undercooled alloys, *Acta Metallurgica*, 1987, **35,** 957–964.
23. Mullins, W. W. and Sekerka, R. F., Stability of a planar interface during solidification of a dilute binary alloy. *Journal of Applied Physics*, 1964, **35,** 444–451.
24. Willnecker, R., Herlach, D. M. and Feuerbacher, B., Evidence of non-equilibrium processes in rapid solidification of undercooled melts. *Physics Review Letters*, 1989, **62,** 2707–2710.
25. Bassler, B., Hofmeister, W. H., Carro, G. and Bayuzick, R. J., The velocity of solidification in highly undercooled nickel. *Metallurgy and Material Transactions*, 1994, **25A,** 1301–1308.
26. Shiraishi, Y. and Tsu, Y., The 140th Committee, The Japan Society for the Promotion of Science (JSPS) Rep. No. 129, 1982.
27. Schwarz, M., Karma, A., Eckler, K. and Herlach, D. M., Physical mechanism of grain-refinement in solidification of undercooled melts. *Physics Review Letters*, 1994, **73,** 1380–1383.
28. Kubaschewski, O. and Alcock, C. B., *Metallurgical Thermochemistry*, 5th edn. Pergamon Press, Oxford, 1979.
29. Steinberg, D. J., A simple relationship between the temperature dependence of the density of liquid metals and their boiling temperature. *Metallurgy Transactions*, 1974, **5,** 1341–1343.
30. Zinov'yev, V. Ye., Polev, V. F., Taluts, S. G., Zinov'yeva, G. P. and Il'iykh, S. A., Diffusivity and thermal conductivity of 3D-transition metals in solid and liquid states. *Physics of Metals and Metallurgy*, 1986, **61,** 85–92.
31. Waseda, Y. and Miller, J. A., Calculation of the crystal melt interfacial free energy from experimental radial distribution function data. *Transactions of the JIM*, 1978, **19,** 546.